PHILOSOPHICAL TRANSACTIONS OF THE ROYAL SOCIETY A MATHEMATICAL, PHYSICAL & ENGINEERING SCIENCES

Palaeomagnetic Results from the Tibetan Plateau

Lin Jinlu and D. R. Watts

Phil. Trans. R. Soc. Lond. A 1988 **327**, 239-262
doi: 10.1098/rsta.1988.0128

Phil. Trans. R. Soc. Lond. A **327**, 239–262 (1988) [239]
Printed in Great Britain

Palaeomagnetic results from the Tibetan Plateau

By Lin Jinlu[1] and D. R. Watts[2]

[1] *Institute of Geology, Academia Sinica, Beijing, People's Republic of China*
[2] *Department of Geology, University of Glasgow, Glasgow G12 8QQ, U.K.*

Palaeomagnetic measurements were carried out on 1325 oriented samples collected from 246 sites on a traverse of the Tibetan Plateau from Lhasa to Golmud in 1985, crossing the Lhasa Terrane, Qiangtang Terrane, and Kunlun Terrane. High blocking temperature, high coercivity, statistically grouped magnetizations were isolated from the following units: Lhasa Terrane – Cretaceous Takena Formation, mid-Cretaceous Nagqu volcanics, mid-Cretaceous Qelico volcanics; Qiangtang Terrane – Norian Batang Group volcanics, Kimmeridgian Yanshiping Group, Paleocene to Eocene Fenghuoshan Group; Kunlun Terrane – Visean to Namurian Dagangou Formation, dykes of the Triassic igneous province. The Triassic data from the Kunlun Terrane, Triassic and Lower Tertiary data from the Qiangtang Terrane and the Cretaceous data from the Lhasa Terrane indicate palaeolatitudes *ca.* 20° S of their present position within the Eurasian frame of reference. A possible interpretation is that the terranes successively accreted to Eurasia and remained in the southern position until the convergence of India drove them northward via a process of tectonic shortening and/or displacement of continental crust. The Carboniferous data from the Kunlun Terrane are consistent with moderate Southern Hemisphere latitude, well separated from Eurasia which was in the Northern Hemisphere at this time, implying the existence of ocean crust between these blocks during the Carboniferous.

1. Introduction

Palaeomagnetic data are potentially useful for resolving tectonic problems posed by the geodynamic evolution of Asia. The Phanerozoic geological history of southeast Asia has involved lateral translation of continental crust by thousands of kilometres. Although the present process is perhaps better modelled as deformation of a continuum, the past evolution must be described using discrete terranes as this is the only tractable approach, given the decrease of information with the passage of geological time. Palaeomagnetism provides the only quantitative means of determining palaeolatitude and palaeoazimuth of crustal blocks as a function of time in the absence of a marine magnetic anomaly record. Rotations between and within blocks may be detected; but with a small data set it may be difficult to distinguish local rotations from terrane-scale displacements.

For these reasons, palaeomagnetic study was included as a part of the Tibetan Geotraverse. It has been suggested that the plateau is crossed by at least three sutures, separating four terranes (Chang *et al.* 1986), including India, the Lhasa Terrane, the Qiangtang Terrane, and the Kunlun Terrane. It is not yet possible to construct polar wander paths for the last three Tibetan terranes. Local rotations obscure the palaeoazimuth determination. Remagnetization and the rather small stratigraphic range of suitable rock types on each terrane limit the amount of useful palaeomagnetic data that can be gathered. Even without polar wander paths,

measurement of the palaeomagnetic inclination with respect to bedding allows the construction of a time sequence of movement in palaeolatitude, and affinity with one or another of the major continental units can be tested.

2. Method

Table 1 lists the sampling localities, letter designations of samples, age of units, and numbers of samples and sites of the palaeomagnetic collections from the Tibetan Plateau. Figure 1 is a map of the traverse area showing the palaeomagnetic sampling localities labelled with the locality designations given in table 1.

With the exception of twentyfour block samples collected from the Dagze volcanics near Quesongsi, orientated drill cores were taken using a portable petrol-driven drill. Magnetic remanence and susceptibility were measured in the field to evaluate the potential of each lithological unit as a suitable recorder of the palaeomagnetic field. Rocks with konigsberger ratios greater than unity were regarded as especially promising. Orientations were measured with a clinometer, magnetic compass and, when possible, a solar compass.

Table 1. Palaeomagnetic sampling localities

(Listed are the locality designations, place names, latitudes, and longitudes of the sampling localities, geological unit, age, number of samples and number of sites.)

locality	place name	lat.	long.	unit	age	samples	sites
P1	Linzhou	29° 54′	91° 14′	Takena Formation	uK	42	7
P2	Linzhou	29° 57′	91° 09′	Takena Formation	uK	13	2
P3	Maqu	29° 50′	90° 44′	Takena (dolomite)	uK	23	3
P4	Quesongsi	30° 00′	90° 44′	Dagze volcanics	Tr	24	8
P5	Damxung	30° 32′	91° 03′	limestone	uC	25	2
P6	Damxung	30° 32′	91° 03′	mixtite	uC	8	1
P7	Nagqu	31° 29′	91° 49′	Diorite	?	6	1
P8	Nagqu	31° 29′	92° 02′	andesites	(96 Ma)	61	9
P9–10	Qelico	31° 42′	90° 57′	andesites	(90 Ma)	42	7
P11	Jang Co	31° 30′	90° 54′	gabbro	?	36	6
P12	Jang Co	31° 28′	90° 40′	mixtite	uC	46	9
P13	Dongqiao	31° 55′	90° 51′	Jienong Formation	mJ	11	2
P14	Tojiu Pass	32° 33′	91° 51′	Yanshiping Group	mJ	41	7
P15	114 station	32° 26′	91° 48′	flysch	mJ	33	6
P16–18	Amdo	32° 13′	91° 29′	Takena Formation	uK	62	10
P19	Yanshiping	33° 36′	92° 04′	Yanshiping Group	mJ	104	17
P20	Yanshiping	33° 34′	92° 03′	Yanshiping Group	mJ	31	6
P21	Kaixinling	34° 08′	92° 23′	Kaixinling Group	uP	51	8
P22	Kaixinling	34° 06′	92° 23′	Kaixinling Group	uP	43	7
P23	Erdaogou	34° 34′	92° 42′	Fenghuoshan Group	Pal-Eo	87	20
P24	Erdaogou	34° 37′	92° 47′	Fenghuoshan Group	Pal-Eo	72	20
P25	Yaxico	34° 19′	93° 28′	Batang Group	uTr	39	6
P26	Xiaonamchuan	35° 51′	94° 21′	volcanics	uTr	29	5
P27	Xiaonamchuan	35° 48′	94° 21′	volcanics	uTr	14	2
P28	Kunlun pass	35° 38′	94° 04′	lake varves	Q	1	1
P29	Yeniuqou	35° 52′	94° 20′	volcanics	P?	26	4
P30–31	Xidatan	35° 46′	94° 20′	Xidatan granite	?	49	8
P32	816 station	36° 10′	94° 47′	andesite dykes	240 Ma	80	22
P33	Dongdatan	35° 47′	94° 58′	redbeds	?	21	3
P34	823 station	36° 05′	94° 49′	volcanics	D	29	5
P35–36	823 station	36° 03′	94° 51′	volcanics	C?	49	9
P37–38	823 station	36° 05′	94° 49′	volcanics	D	33	6
P39–40	Dagangou	36° 02′	95° 00′	Dagangou Formation	C	48	9
P41	Dagangou	36° 02′	95° 00′	Dagangou Formation	C	24	4
P42–43	Golmud	36° 13′	94° 43′	andesite dykes	240 Ma	22	4

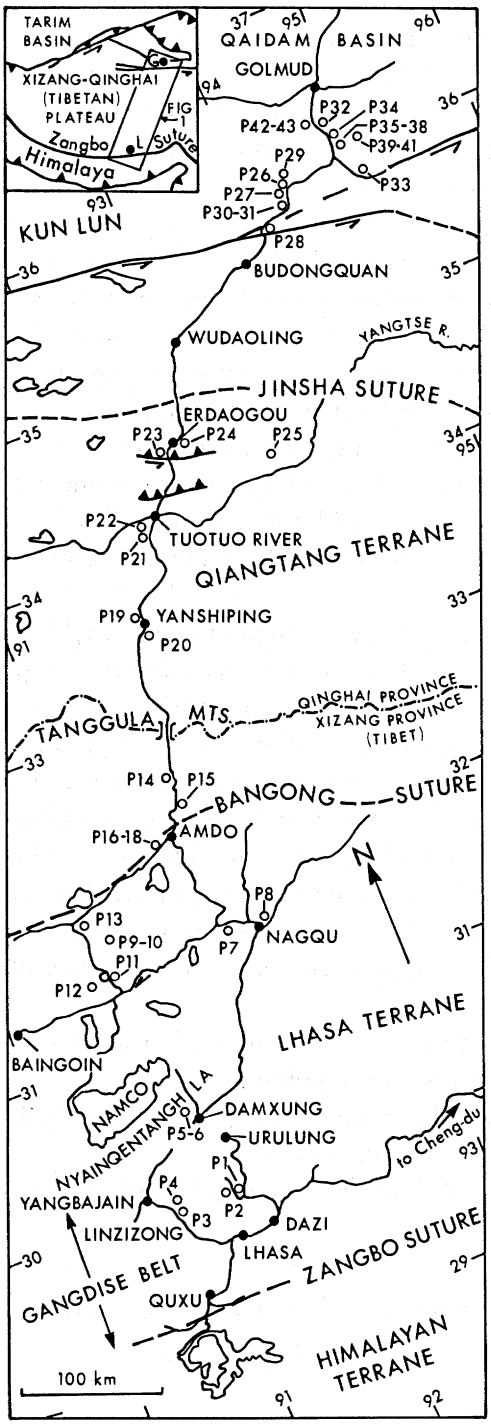

FIGURE 1. Map of Geotraverse area of Tibet showing palaeomagnetic sampling localities, P1–P43.

Samples were cut into cylindrical specimens 2.5 cm in diameter and 2.3 cm high. Magnetic measurements were carried out at the University of Leeds (L.J.L.) using a cryogenic magnetometer and fluxgate spinner magnetometer, and at the University of Glasgow (D.R.W.) with a fluxgate spinner magnetometer. The error of individual measurements was determined at each stage. Alternating field demagnetizations were carried out with a tumbler device

(McElhinny 1966) at Leeds, and a three axis, static, microcomputer-controlled demagnetizer working at 186 Hz at Glasgow. Thermal demagnetizations were carried out with a Helmholtz coil nulled oven (McElhinny *et al.* 1971) at Leeds and a microcomputer-controlled bench type, mu-metal shielded oven at Glasgow. Selected redbed samples were chemically demagnetized by cutting slices in the specimens and immersing them in 8 N HCl with the earth's field nulled by mu-metal boxes. Each specimen was demagnetized in detail. The behaviour of the magnetization was continuously monitored using orthogonal projections (Zijderveld 1967), displayed after each step. In some cases, alternating field demagnetization failed to remove a significant percent of the magnetization after a maximum field treatment. The investigation of such samples was continued using thermal demagnetization.

The final evaluation of the component structure of each specimen was done using orthogonal projections interactively with the principal component analysis algorithm of Kent *et al.* (1983) which utilizes the individual errors of measurement. Data were exchanged between Leeds and Glasgow via computer tape and the JANET network. Principal component directions and intensities were written into computer files which were edited, isolating magnetizations with similar directions and physical properties. Mean site directions and statistics were computed from these files.

Analysis analogous to the great circle method of Halls (1978) was also employed. The Kent *et al.* algorithm fits planes as well as lines to distributions of points in a demagnetization sequence. For each data set, the poles to the best-fitting planes were written into a computer file, plotted on an equal area projection and examined for great circle distributions. The pole of this great circle is the direction of magnetization that is common to all of the planes and is identical to the direction that would be identified by converging demagnetization circles.

The properties of the magnetization, mean site directions and associated statistics for those lithological units which have a palaeomagnetic signal are discussed in turn, according to the terrane in which they are found. A number of units listed in table 1 were found to have magnetizations with the following properties and are not representative of the palaeomagnetic field:

1. magnetizations which displayed random walk trajectories on orthogonal projections without linear or planar distribution of points;

2. magnetizations with low blocking temperature (generally less than 200 °C and/or low blocking fields (generally less than 100 oersted);

3. magnetizations with a random distribution (estimate of Fisher's precision parameter, k, less than 4).

3. Properties and directions of magnetization

(*a*) *Lhasa Terrane*

(i) *Takena Formation* (P1, P2)

Fine-grained sandstone and siltstone were sampled from two localities, P1 and P2, near Linzhou. The two sections have different attitudes and therefore allow a fold test. A heavy mineral seam 10 cm thick was collected from section P1, site T7.

The problem of the age of this unit is discussed by Smith & Xu (this volume) and is typical of the difficulty posed by continental redbeds. Following Smith & Xu, the age of the redbed member of the Takena Formation is taken to be early Upper Cretaceous.

Figure 2 illustrates the behaviour of the magnetization characteristic of these sections.

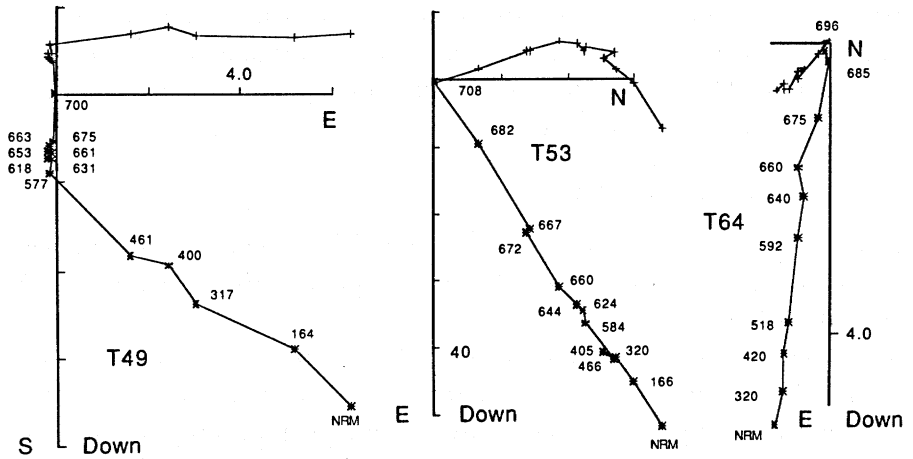

FIGURE 2. Orthogonal projections of thermal demagnetization results from the Takena Formation redbeds. Asterisks denote the intersection of the magnetization vector with the vertical plane, crosses denote the intersection with the horizontal plane. Units of the axes are amp/metre $\times 10^{-3}$.

Specimens T49 and T64 are typical fine-grained red sandstones. Specimen T53 was collected from the heavy mineral seam. The magnetization deemed representative of the palaeomagnetic field is the high blocking temperature component revealed between demagnetization temperatures of 630–660 °C at the lower end of the range and up to 696–708 °C. In many specimens this component was revealed between a narrow range of temperatures near the Neel temperature of hematite as illustrated by T53 and T64. The heavy mineral seam has the same palaeomagnetic signature as the fine sandstone but the NRM (natural remanent magnetization) intensities are 40 mamp/metre, about an order of magnitude greater than the sandstone at 4 mamp/metre.

The mean site directions, associated statistics, pole positions and palaeolatitudes derived from the Takena Formation, before and after structural correction, are summarized in table 2.

TABLE 2. TAKENA FORMATION: MEAN SITE DIRECTIONS, STATISTICS, POLE POSITIONS AND PALAEOLATITUDES

(The parameters are given before (left columns) and after (right columns) structural correction. *N* is the number of samples/sites from which a determination is made; *Dec* is the mean declination; *Inc* is the mean inclination; *k* is the estimate of Fisher's precision parameter; alpha95 is the apical half angle of the cone of 95% confidence; dp is the estimate of the error of the palaeolatitude; dm is the estimate of the error of palaeoazimuth.)

Unit: Takena Formation (P1, P2)
Age: uK
Location: Linzhou (29° 54′, 91° 14′; 29° 57′, 91° 09′)

site	*N*	*Dec*	*Inc*	*k*	alpha95	*Dec*	*Inc*	*k*	alpha95
T01	4	19	48	58	12.1	6	15	59	12.1
T02	4	17	48	52	12.9	5	15	52	12.9
T03	7	19	45	47	8.9	7	12	47	8.9
T04	6	358	53	42	10.5	351	17	42	10.5
T05	10	6	49	19	11.5	357	14	19	11.5
T06	6	343	54	375	3.5	338	11	375	3.5
T07	6	28	85	9	23.0	355	17	9	23.0
T08	8	13	87	32	10.0	355	15	32	10.0
Mean	8	8	59	19	13.0	357	15	70	6.7

Pole: lat = 78, long = 123,
dp = 14.5, dm = 22.5
Palaeolatitude: = 39.8 ± 14.5°

Pole: lat = 68°, long = 279°
dp = 3.5, dm = 6.9
Palaeolatitude: = 7.6 ± 3.5°

The directions of magnetization have the smallest dispersion after structural correction, passing the fold test at the 99% level of confidence. Secondary magnetizations are present and are thermally distributed but do not define a meaningful population. This reproduces the results of Achache *et al.* (1984) for this formation.

(ii) *Nagqu mid-Cretaceous volcanics* (P8)

This section, P8, comprises andesites interbedded with basalts of the mid-Cretaceous volcanic province (see Pearce & Mei, this volume). In the Nagqu area, these rocks have $^{40}Ar/^{39}Ar$ ages between 100 and 95 Ma.

Typical response to demagnetization is shown by the orthogonal projections in figure 3. Specimen ZN15a is subjected only to thermal demagnetization. The orthogonal projection reveals a high blocking temperature, thermally discrete magnetization removed between 532 and 641 °C. Specimens ZN27a and ZN45a were treated by alternating field demagnetization, followed by thermal demagnetization. The characteristic magnetization is only partially removed by alternating fields up to 1000 oersted. No persistent, statistically viable secondary magnetizations were found.

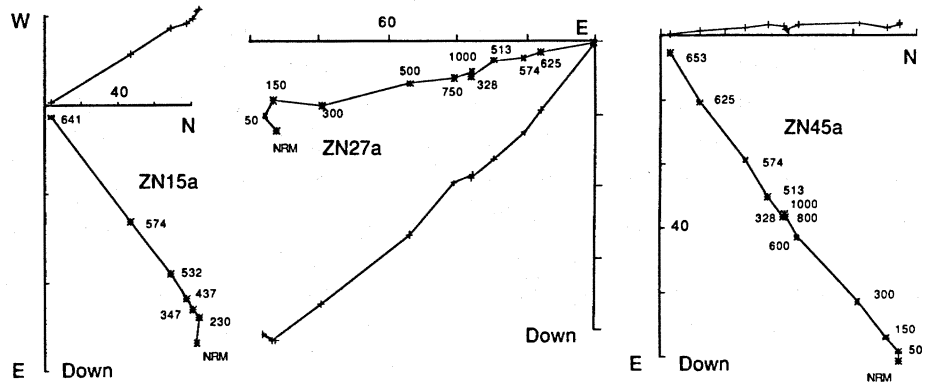

FIGURE 3. Orthogonal projections of thermal and alternating field demagnetization results from the Nagqu mid-Cretaceous volcanics. Convention of plotting is as in figure 2.

Table 3 summarizes the mean site directions, statistics, pole positions and palaeolatitude estimates, before and after structural correction. The estimate of Fisher's (1953) precision parameter, k, drops from 74 to 54 after structural correction. This may either reflect a remagnetization or an imprecise attitude determination of the individual sites. The measurement of the strike and dip of this section is difficult as the indicators of bedding are vague and equivocal. The structurally corrected mean direction reproduces the result of Achache *et al.* (1984), who noted that the mean direction of magnetization seems anomalously steep compared to other units with the same age. This may be related to the difficulty of determining a precise structural attitude from this locality.

(iii) *Qelico section, mid-Cretaceous volcanics* (P9, P10)

Oriented core samples were collected from the andesites of the north Lhasa Terrane mid-Cretaceous volcanic province (Pearce & Mei, this volume) from localities P9 and P10. At P9 the andesites underlie redbeds of probable Cretaceous age. $^{40}Ar/^{39}Ar$ ages are between 95 and 85 Ma near these localities (Coulon *et al.* 1986).

Specimens from this unit showed two types of response to demagnetization as shown in figure 4. The response which reveals the palaeomagnetic signal is illustrated by projections of demagnetizations of specimens QL01a and QL03. Thermal demagnetization removes a thermally distributed secondary magnetization to reveal a high blocking temperature magnetization which is taken to be a record of the palaeomagnetic field. This magnetization has

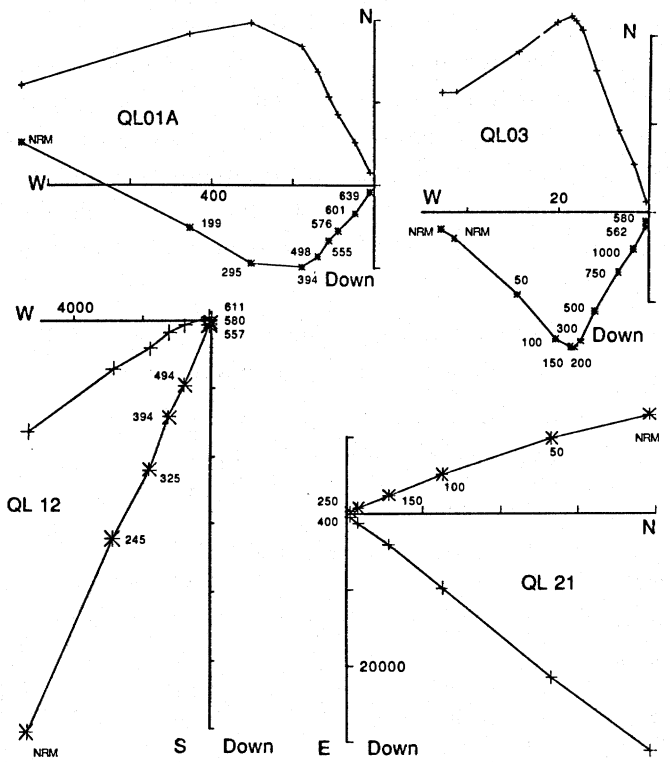

FIGURE 4. Orthogonal projections of thermal and alternating field demagnetization results from the Qelico mid-Cretaceous volcanics. Convention of plotting is as in figure 2.

TABLE 3. NAGQU SECTION OF MID-CRETACEOUS VOLCANICS: MEAN SITE DIRECTIONS, STATISTICS, POLE POSITIONS AND PALAEOLATITUDES

(The arrangement and parameters are as in table 2.)

Unit: Nagqu Cretaceous Andesites (P8)
Age: Cretaceous 96 Ma
Location: Nagqu (31° 29′, 92° 02′)

site	*N*	*Dec*	*Inc*	*k*	alpha95	*Dec*	*Inc*	*k*	alpha95
ZN01	4	314	54	354	4.9	354	38	352	4.9
ZN02	4	321	59	573	3.8	2	38	584	3.8
ZN03	5	323	52	344	4.1	357	33	345	4.1
ZN04	5	325	52	930	2.5	358	32	929	2.5
ZN06	3	314	50	713	4.6	350	36	724	4.6
ZN07	4	353	57	128	8.1	16	26	128	8.1
ZN08	2	338	57	1020	7.8	8	31	1062	7.7
ZN09	3	307	47	350	6.6	344	38	346	6.6
ZN10	3	310	50	509	5.5	348	38	506	5.5
Mean	9	322	54	74.3	6.0	358	35	54	6.0
		Pole: lat = 58, long = 18				Pole: lat = 78, long = 282			
		$dp = 5.9$, $dm = 8.4$				$dp = 4.0$, $dm = 6.9$			
		Palaeolatitude: 35±5.9°				Palaeolatitude: 19±4.0°			

blocking temperatures between 498 and 639 °C. Alternating field demagnetization removes the secondary magnetization at about 200 oersted, and a part of the characteristic magnetization is removed at higher fields, up to 1000 oersted. Thermal demagnetization completes the removal of the characteristic magnetization as illustrated by QL03.

The second type of behaviour is illustrated by thermal demagnetization of QL12 and alternating demagnetization of QL21. Such samples are strongly magnetized with NRMs at least an order of magnitude greater than samples with the previous type of magnetization. This second behaviour is characterized by a univector appearance on the orthogonal projection and thermally distributed response as shown by QL12. This type of magnetization is also quickly removed by alternating field demagnetization with 99% of the NRM removed at 400 oersted.

The thermally distributed, low blocking temperature magnetization has a high between-site dispersion. This population of magnetizations may be due to lightning strikes or to large multi-domain carriers of magnetization. The mean directions in table 4 for this unit are calculated

TABLE 4. QELICO SECTION OF MID-CRETACEOUS VOLCANICS: MEAN SITE DIRECTIONS, STATISTICS, POLE POSITIONS AND PALAEOLATITUDES

(The arrangement and parameters are as in table 2.)

Unit: Andesite Volcanics (P9–10)
Qelico, near Jang Co (31° 42′, 90° 57′)
Age: 90 Ma

site	*N*	*Dec*	*Inc*	*k*	alpha95	*Dec*	*Inc*	*k*	alpha95
QL01	5	337	30	825	2.7	350	24	835	2.6
QL02	4	343	36	35	15.8	358	28	35	15.8
QL03	3	16	−49	3	84.9	343	−62	3	84.9
QL04	5	32	−20	21	17.1	24	−41	21	17.1
QL05	5	212	73	716	2.9	97	77	711	2.9
QL06	4	319	49	36	15.5	348	47	35	15.7
QL07	7	327	59	360	3.2	331	42	366	3.2
Mean	4	333	44	29.4	17.2	347	36	32	16.5
		Pole: lat = 65, long = 354				Pole: lat = 74, long = 318			
		$dp = 13.5$, $dm = 21.6$				$dp = 11.1$, $dm = 19.1$			
		Palaeolatitude: $25.8 \pm 13.5°$				Palaeolatitude: $19.8 \pm 11.1°$			

exclusively from the high blocking temperature thermally discrete magnetizations first described. The two localities have different attitudes; structural correction increases the k of the population of the discrete magnetizations, but the increase is not statistically significant.

(*b*) *Qiangtang Terrane*

(i) *Batang Group volcanics* (P25)

This section of andesite–basalt lavas is described by Pearce & Mei (this volume). The age is determined by the Norian marine carbonates that conformably overlie these rocks (Smith & Xu, this volume).

Figure 5 shows orthogonal projections that summarize the response to thermal and alternating field treatment. Specimens QT2 and QT4 illustrate nearly univector magnetizations with blocking fields up to 1800 oersted and blocking temperatures between 529 and 572 °C. As illustrated by QT16 and QT38, a number of specimens have significant secondary magnetizations that dominate the NRM. These secondary magnetizations are removed at 600 oersted

and 434 °C to reveal the characteristic magnetization with the same direction as the high blocking field, thermally discrete univector magnetizations.

The mean site directions, statistics, pole positions, and estimates of palaeolatitude are summarized in table 5, before and after structural correction. The section has a substantial dip, but the attitude of the volcanics is well-determined by the overlying bedded marine carbonates. Unfortunately only the one limb of the structure could be sampled so a fold test is not possible.

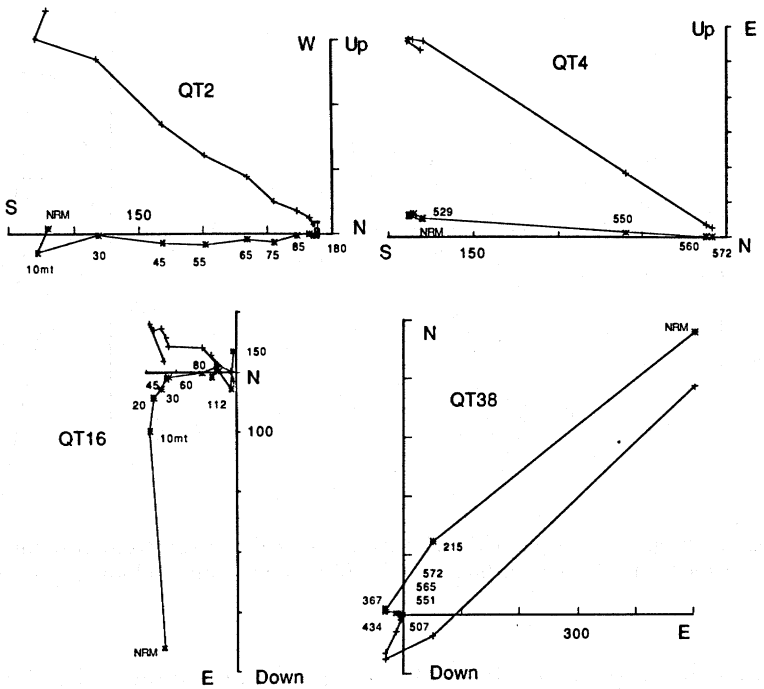

FIGURE 5. Orthogonal projections of thermal and alternating field demagnetization results from the Batang Group volcanics. Convention of plotting is as in figure 2.

TABLE 5. BATANG GROUP VOLCANICS: MEAN SITE DIRECTIONS, STATISTICS, POLE POSITIONS AND PALAEOLATITUDES

(The arrangement and parameters are as in table 2.)

Unit: Batang Group volcanics (P25)
Location: Yaxico (34° 19′, 93° 28′)
Age: Norian (205 Ma)

site	*N*	*Dec*	*Inc*	*k*	alpha95	*Dec*	*Inc*	*k*	alpha95
QT01	6	215	−2	281	4.0	234	−58	282	4.0
QT02	6	223	18	23	14.2	228	−36	23	14.2
QT03	6	204	13	53	9.3	207	−47	53	9.3
QT04–05	7	192	27	4	35.0	192	−34	4	35.0
QT06	9	210	−2	90	5.5	224	−60	90	5.5
Mean	5	209	11	23	16.2	215	−48	23	16.2
		Pole: lat = 42°, long = 234°				Pole: lat = 59°, long = 184°			
		$dp = 8.3°$, $dm = 16.4°$				$dp = 13.8°$, $dm = 21.2°$			
		Palaeolatitude: $-6 \pm 8.6°$				Palaeolatitude: $29 \pm 13.8°$			

(ii) *Yanshiping Group* (P19, P20)

The Yanshiping Group is an extensive sequence of redbeds 2 kilometres thick with occasional marine incursions of Bathonian to Kimmeridgian age (Smith & Xu, this volume). Two localities, P19 and P20, were sampled. P19 is a vertical sequence of redbeds along the road in and just north of Yanshiping. P20 is a moderately dipping section of limestones interbedded with red sandstones about 3 kilometres south of Yanshiping.

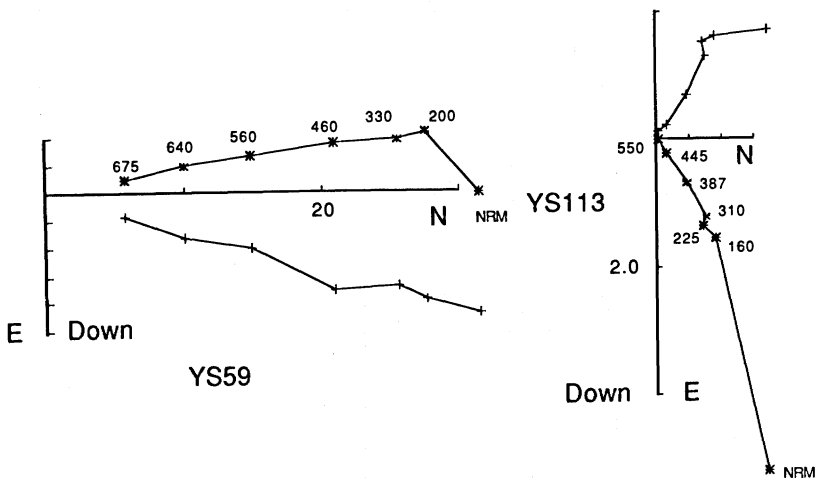

FIGURE 6. Orthogonal projections of thermal and alternating field demagnetization results from the Yanshiping Group redbeds (YS59) and carbonates (YS113). Convention of plotting is as in figure 2.

Figure 6 shows the response to thermal demagnetization typified by the redbed specimen, YS59, and the limestone YS113. The magnetization of the redbeds was nearly univector with low intensity, randomly oriented secondary magnetizations. Blocking temperatures of the redbed magnetization are distributed from 200 to 675 °C. The NRM of the limestone is typically about 4 mamp/metre, about an order of magnitude less than the redbeds. Thermal demagnetization of the limestone revealed a distributed magnetization with maximum blocking temperatures up to 550 °C. The carrier of the magnetization in the redbeds is likely to be hematite and in the limestone, magnetite.

The mean site directions of these magnetizations from the Yanshiping Group are given in table 6. Figure 7 shows two equal area projections of the total population of magnetization directions. Although there is a significantly lower dispersion after structural correction, the lowest dispersion actually occurs at an intermediate state. Figure 8 is a plot of the estimate k, of Fisher's precision parameter of the total distribution as a function of the percentage of the total structural correction. The maximum k at an intermediate stage in the structural correction indicates that the magnetization in either or both localities was acquired during the folding of this sequence. This demonstration shows that the palaeomagnetic record from these rocks is useless as an indicator of palaeolatitude. If the magnetization was acquired during the folding, bedding is no longer representative of palaeohorizontal.

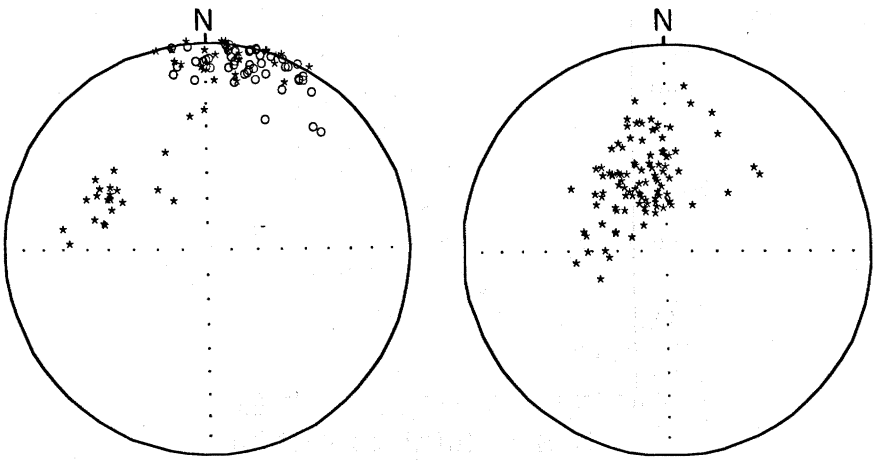

FIGURE 7. Equal area projections of Yanshiping Group characteristic directions of magnetization before (left) and after (right) structural correction. Asterisks denote intersection with the lower hemisphere. Circles denote intersection with the upper hemisphere.

TABLE 6. YANSHIPING GROUP: MEAN DIRECTION, STATISTICS, POLE POSITIONS AND PALAEOLATITUDES

(The arrangement and parameters are as in table 2. Sites YS01–YS15 were collected from locality P19. Sites YS16–YS23 were collected from locality P20.)

Unit: Yanshiping Group (P19, P20)
Age: Bathonian to Kimmeridgian (145–166 Ma)
Location: (33° 36′, 92° 04′)

site	*N*	*Dec*	*Inc*	*k*	alpha95	*Dec*	*Inc*	*k*	alpha95
YS01	7	4	14	148	4.9	275	61	148	4.9
YS02	8	358	−5	81	6.2	313	56	81	6.2
YS03	5	356	4	46	11.4	315	57	36	12.9
YS04	8	17	0	81	6.2	352	66	79	6.3
YS05	6	15	−7	125	6.0	356	62	125	6.0
YS06	7	10	0	206	4.2	325	69	206	4.2
YS07	6	15	−3	43	10.4	329	64	43	10.4
YS08	8	23	−6	123	5.0	346	69	123	5.0
YS09	9	16	−4	48	7.5	328	61	48	7.5
YS10–11	3	359	0	38	20.3	325	56	38	20.2
YS12	4	357	7	13	26.2	308	61	14	25.6
YS13	5	30	−22	27	14.9	35	49	27	14.9
YS14	3	357	−15	72	14.6	344	50	72	14.6
YS15	4	5	11	24	19.1	297	72	24	19.1
YS16	3	295	45	13	35.6	348	39	13	35.6
YS17–18	4	299	48	30	16.9	352	37	30	16.9
YS19–20	3	301	43	11	39.0	345	38	12	36.5
YS21	5	294	44	161	6.0	352	43	161	6.0
YS22	3	292	40	96	12.7	349	45	101	12.3
YS23	3	287	45	161	9.7	355	48	161	9.8
Mean	20	353	14	4.5	17.4	339	58	21.3	7.2
		Pole: lat = 63, long = 287				Pole: lat = 72, long = 25			
		$dp = 9.1$, $dm = 17.8$				$dp = 7.8$, $dm = 10.6$			
		Palaeolatitude:				Palaeolatitude: = 39 ± 7.8°			

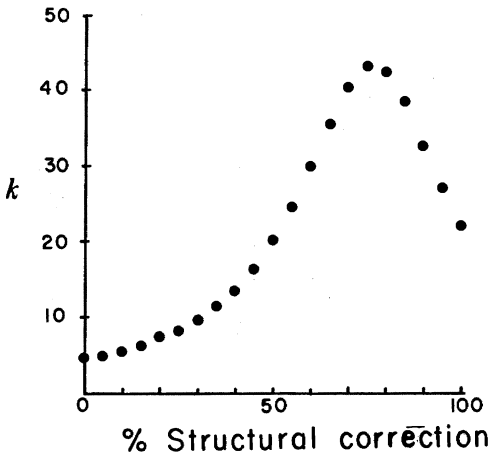

FIGURE 8. Plot of the estimate of Fisher's precision parameter, k, against percent of structural correction for the Yanshiping Group characteristic directions of magnetization.

(iii) *Fenghuoshan Group* (P23, P24)

The Fenghuoshan Group is a thick sequence of continental redbeds with thin lacustrine limestones yielding a fauna of Palaeocene to early Eocene age. These sediments form monotonously dipping sequences riding on thrust faults. Two sections were sampled from this Group at localities P23 and P24.

Figure 9 illustrates the typical response to demagnetization experiments of the samples collected from locality P23. The sister specimens FH15a and FH15b, from the same sample, were treated by chemical and thermal demagnetization methods respectively. Comparison of

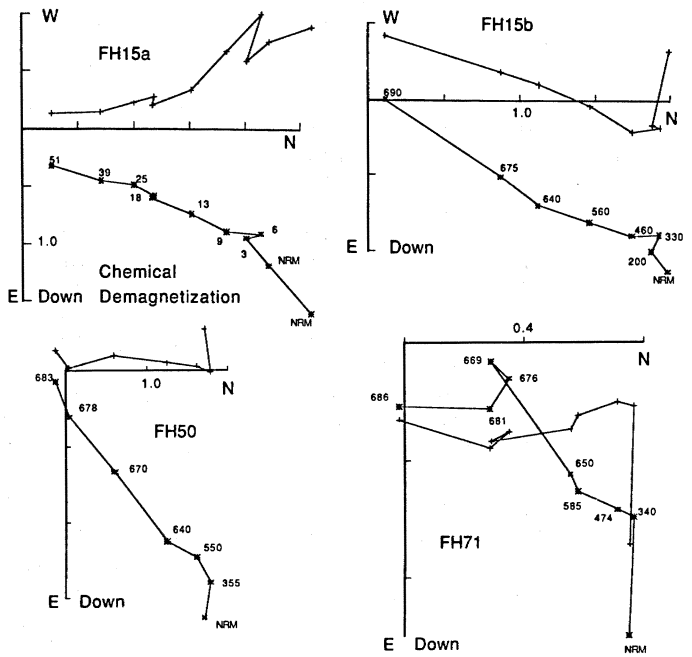

FIGURE 9. Orthogonal projections of chemical and thermal demagnetization results from the Fenghuoshan Group redbeds, locality P23. Convention of plotting is as in figure 2.

the response using orthogonal projections shows that chemical leaching simultaneously removes a secondary magnetization and a more stable magnetization. Thermal demagnetization quickly removes the secondary component to reveal a high blocking temperature thermally discrete magnetization that has a linear trajectory but does not move directly toward the origin of the diagram. At the last stages of treatment the magnetizations were very weak, near the sensitivity of the cryogenic magnetometer, and the errors of the individual measurements were greater than 10°. It was not possible to isolate a component of magnetization near the origin of the orthogonal projections. In the case of FH71 the characteristic magnetization is revealed between steps of 585 and 669 °C.

TABLE 7. FENGHUOSHAN GROUP: LOCALITY P23, MEAN SITE DIRECTIONS, STATISTICS, POLE POSITIONS AND PALAEOLATITUDES

(The arrangement and parameters are as in table 2.)

Unit: Fenghuoshan Group (P23)
Age: Palaeocene–Eocene
Location: Erdaogou (34° 34′, 92° 23′)

site	*N*	*Dec*	*Inc*	*k*	alpha95	*Dec*	*Inc*	*k*	alpha95
FH01	7	352	64	12	18.2	351	17	12	18.2
FH02	6	18	59	17	16.8	5	15	17	16.8
FH03	8	359	33	14	15.0	1	−10	14	15.0
FH04	9	20	52	39	8.3	15	8	37	8.6
FH05	5	69	64	69	9.3	33	31	69	9.3
FH06	6	38	57	8	25.5	15	20	8	25.5
FH07	6	38	39	96	6.9	25	4	96	6.9
FH08	5	30	62	71	9.2	16	24	70	9.2
FH09	6	15	51	79	7.6	10	12	79	7.6
FH10–11	3	15	64	35	21.1	0	20	35	21.1
FH12	3	20	49	61	15.9	9	8	61	15.9
FH13–14	7	41	58	10	19.9	21	20	10	19.6
FH15	5	12	55	24	15.9	6	13	2	16.0
FH18	4	347	52	118	8.5	352	5	117	8.5
FH19	4	28	63	104	9.1	2	24	103	9.1
Mean	15	20	56	31	6.9	9	14	29	7.2
		Pole: lat = 73, long = 169				Pole: lat = 61, long = 253			
		$dp = 7.2$, $dm = 10.0$				$dp = 3.8$, $dm = 7.4$			
		Palaeolatitude: = 36.9 ± 7.2°				Palaeolatitude: = 7.3 ± 3.8°			

Table 7 summarizes the mean site directions, associated statistics and pole positions, before and after structural correction. All of the high blocking temperature magnetizations are of normal polarity and the mean direction, computed from all of the sites, is near the present-day field direction for this site, before structural correction is applied. The structural correction takes the mean direction of magnetization to a shallow inclination.

Figure 10 shows the results of thermal demagnetizations of specimens from locality P24, near Erdaogou. Chemical demagnetization was not successful because of the high carbonate content of these sandstones. Typical responses to thermal demagnetization are shown in specimens FE03, FE04, FE06 and FE28. The demagnetization trajectory does not move toward the origin of the orthogonal projections, and in some cases, moves past the origin, into another quadrant. Repeated, closely-stepped, thermal treatment usually failed to reveal the direction of the higher blocking temperature magnetization. However, a component is shown in most specimens from this section, isolated between 350 °C to, generally, 580 °C. The upper limit of the temperature

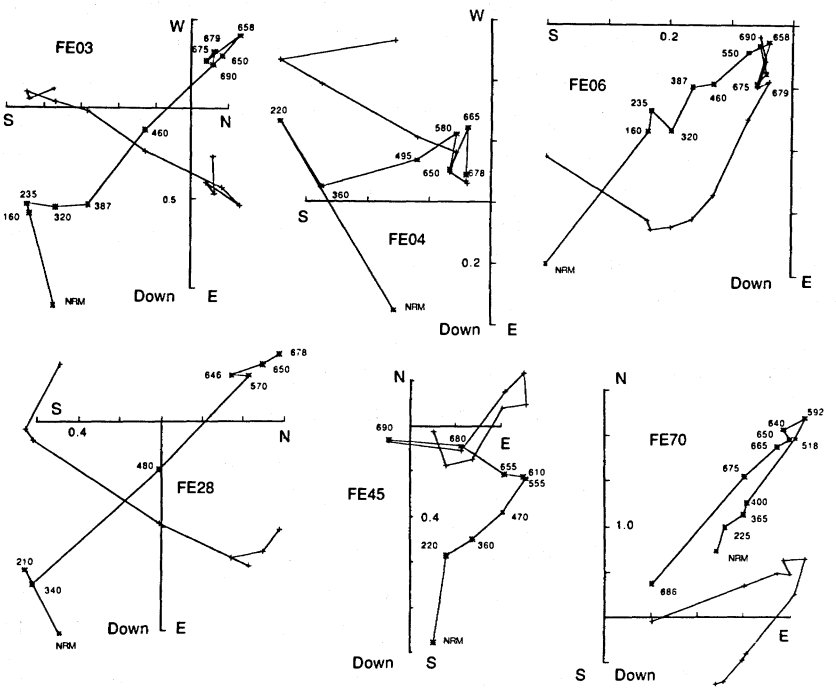

FIGURE 10. Orthogonal projections of thermal demagnetization results from the Fenghuoshan Group redbeds, locality P24. Convention of plotting is as in figure 2.

does vary, sometimes persisting up to 660 °C. Examination of each result depicted in figure 10 shows a component of magnetization with blocking temperatures in a range consistent with magnetite or titantomagnetite as a carrier. FE45 shows this magnetite-carried component superimposed on complex behaviour at temperatures higher than 555 °C. Only rarely is the highest blocking temperature magnetization revealed as illustrated by FE70. The magnetite-carried remanence is shown in this specimen as the lower blocking temperature component between treatments of 365 and 592 °C.

Table 8 lists the mean site directions, statistics and pole positions and palaeolatitudes of the lower-blocking temperature magnetization which is all that can be isolated by detailed demagnetisation experiments on specimens from this section. The population of the high-blocking temperature magnetization such as exhibited by specimen FE70, is too sparse for a meaningful average to be calculated.

The mean direction of the lower-blocking temperature magnetization is southwest and down before structural correction. The tilt correction of the uniformly dipping section takes the mean to a southeast and up direction which could be representative of a Tertiary reversed palaeomagnetic field. In neither case, before or after the structural correction, is this a present day field direction.

The lower-blocking temperature magnetization may not necessarily be an overprint. It could be an early magnetization carried either by detrital or early diagentic magnetite with an overprint carried by later developed hematite.

Figure 11 is an equal area projection of the directions of magnetization from the two sections of the Fenghuoshan Group that were collected, before and after structural correction. Structural correction carries the distribution of magnetizations into a somewhat normal and

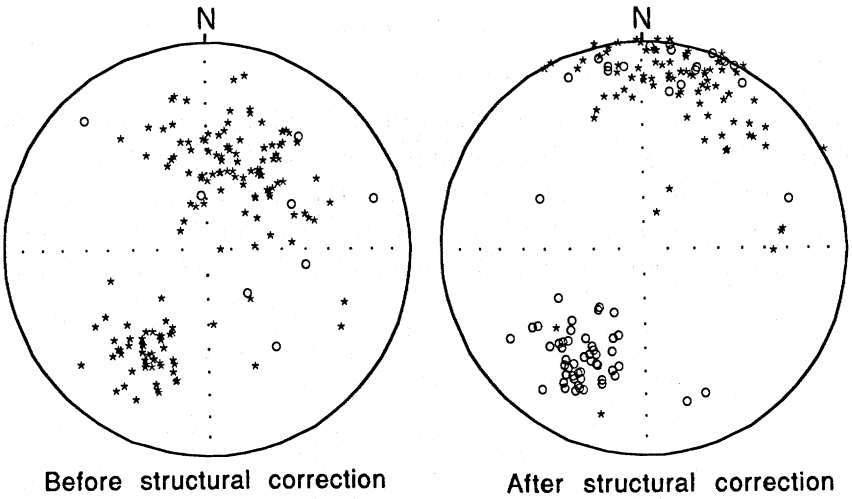

FIGURE 11. Equal area projection of Fenghuoshan Group characteristic magnetization directions before (left) and after (right) structural correction. Convention of plotting is as in figure 7.

TABLE 8. FENGHUOSHAN GROUP: LOCALITY P24, MEAN SITE DIRECTIONS, STATISTICS, POLE POSITIONS AND PALAEOLATITUDES

(The arrangement and parameters are as in table 2.)

Unit: Fenghuoshan Group (P24)
Age: Palaeocene–Eocene
Location: Erdaogou (34° 34′, 92° 47′)

site	*N*	*Dec*	*Inc*	*k*	alpha95	*Dec*	*Inc*	*k*	alpha95
FE01	3	226	58	15	32.9	217	−23	15	32.9
FE02	6	215	29	20	15.3	218	−50	20	15.3
FE03	3	232	43	8	46.3	227	−31	8	46.3
FE04–07	6	224	35	9	24.5	225	−38	9	23.4
FE08–09	6	210	38	50	9.6	210	−35	37	11.2
FE10–12	8	203	36	25	11.4	203	−38	25	11.4
FE13–14	4	223	35	46	13.6	223	−36	50	13.1
FE16	3	213	47	96	12.6	213	−30	97	12.6
FE17	8	214	46	54	7.6	214	−31	54	7.6
FE18	3	210	50	65	15.4	211	−30	86	13.4
FE19	3	207	42	124	11.1	207	−30	124	11.1
FE20	4	209	40	70	11.0	209	−32	71	11.0
Mean	12	215	42	64	5.5	215	−34	79	4.9

Pole: lat = −22, long = 58
$dp = 4.1$, $dm = 6.8$
Palaeolatitude: = −24 ± 4.1°

Pole: lat = 55, long = 201
$dp = 3.2$, $dm = 5.6$
Palaeolatitude: = 18.4 ± 3.2°

reversed distribution, but the mean directions of the two populations are not antipodal. The mean of the normal magnetizations has a distinguishably shallower inclination than the mean of the reversed population. Because the two populations of magnetization are distinct, in terms of their polarity, physical properties and mean directions, they are treated separately for the purpose of calculating the pole positions and estimating palaeolatitudes.

(c) *Kunlun Terrane*

(i) *Dagangou Formation* (P39–40, P41)

The Dagangou Formation is found in the northern Kunlun Mountains, comprising several kilometres of red siltstones, sandstones and arkoses conformably overlain by a marine limestone/shale sequence of latest Visean or early Namurian age (Smith & Xu, this volume).

The siltstone members of this unit were collected at two localities (P39–40 and P41). Typical demagnetization results from P41 are shown in figure 12 and from locality P39–40 in

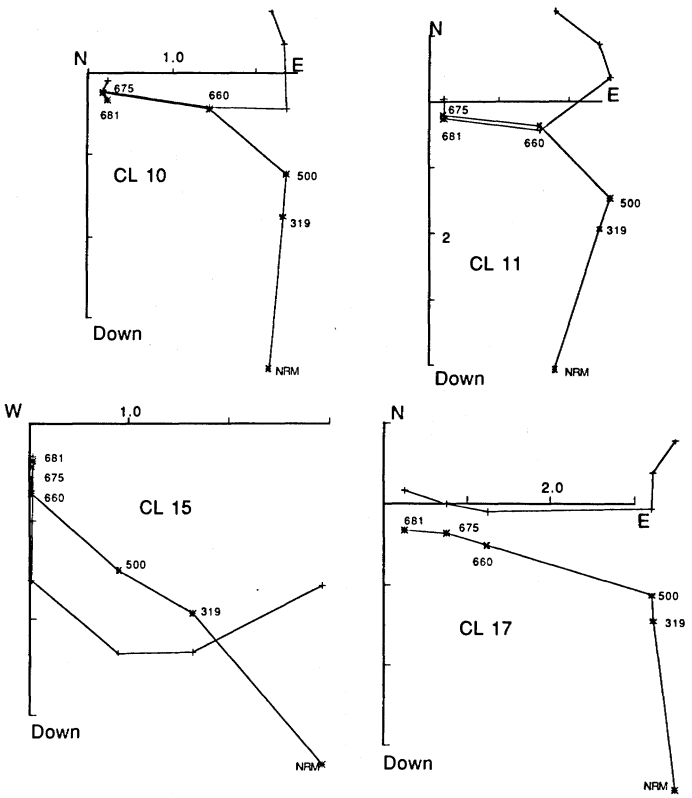

FIGURE 12. Orthogonal projections of thermal demagnetization results from the Dagangou Formation, locality P41. Convention of plotting is as in figure 2.

figure 13. The characteristic magnetization from P41 is thermally discrete and revealed between demagnetization steps of approximately 660 to 681 °C. The behaviour was rather more variable in samples from locality P39–40. Secondary magnetizations are common and sometimes dominate the NRM as illustrated by the behaviour of CS48. Even in such samples it was possible to isolate a high blocking temperature magnetization which is characteristic of the Dagangou Formation at this locality. In all samples, the characteristic magnetization has blocking temperatures between 580 and 678 °C.

The mean directions, statistics, pole positions and estimated palaeolatitudes for section P41 are given in table 9, and those derived from P39–40 in table 10. The localities are dealt with separately because the declination of the characteristic magnetization found in section P39–40 is distinguishable from that found in section P41. The inclinations, after structural correction, are the same.

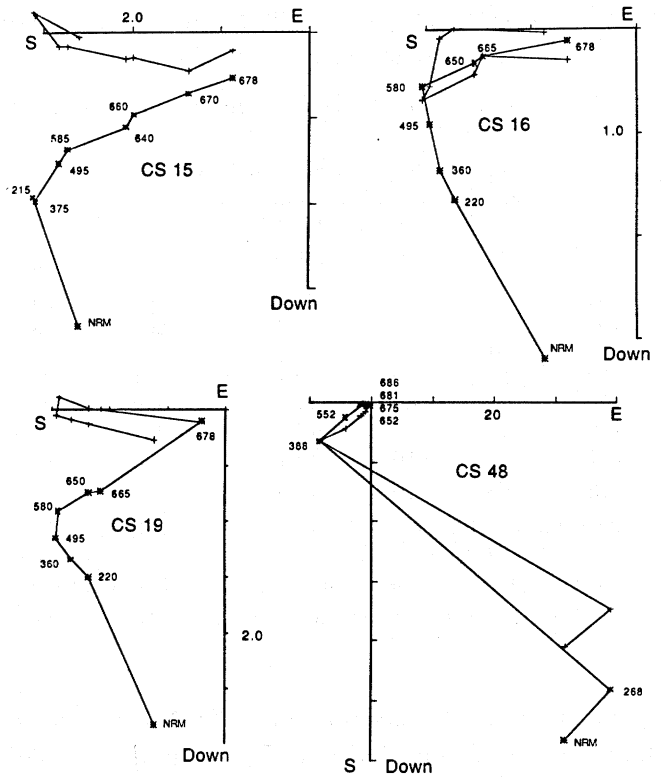

FIGURE 13. Orthogonal projections of thermal demagnetization results from the Dagangou Formation, locality P39–40. Convention of plotting is as in figure 2.

TABLE 9. DAGANGOU FORMATION: LOCALITY P41, MEAN SITE DIRECTIONS, STATISTICS, POLE POSITIONS AND PALAEOLATITUDES

(The arrangement and parameters are as in table 2. The mean direction after correction for a 70° plunge to the west is also given.)

Unit: Dagangou Formation (P41)
Age: Visean to Namurian (325 Ma)
Location: (36° 02′, 95° 00′)

site	*n*	*Dec*	*Inc*	*k*	alpha95	*Dec*	*Inc*	*k*	alpha95
CL01	4	79	29	56	12.3	123	40	56	12.3
CL02	2	89	63	20	59.9	168	44	20	59.9
CL03	6	90	23	15	18.1	119	32	15	18.1
CL04	5	76	23	8	28.8	99	29	8	28.2
Mean	4	83	35	16	23.4	125	39	12	27.8
		Pole: lat = 17, long = 173				Pole: lat = −12°, long = 146°			
		dp = 15.5°, dm = 27.0°				dp = 19.8, dm = 33.2			
		Palaeolatitude: = 19 ± 198°				Palaeolatitude: = −22 ± 19.2°			
		Mean corrected for plunge 70° west:				164	39	12	27.8

Structural evidence suggests that locality P39–40 is on the limb of a fold which is plunging westwards at 70°. No information on a possible plunge of locality P41 is available, but it is interesting to note that if both localities are corrected for a steep plunge to the west, the mean declinations swing around to the south, converging towards each other (see tables 9 and 10).

Other possible explanations for the difference in declination may be local rotations or

TABLE 10. DAGANGOU FORMATION: LOCALITY P39–40, MEAN SITE DIRECTIONS, STATISTICS, POLE POSITIONS AND PALAEOLATITUDES

(The arrangement and parameters are as in table 2. The mean direction after correction for a 70° plunge to the west is also given.)

Unit: Dagangou Formation (P39–40)
Age: Visean to Namurian (325 Ma)
Location: (36° 02′, 95° 00′)

site	*N*	*Dec*	*Inc*	*k*	alpha95	*Dec*	*Inc*	*k*	alpha95
CS01	6	150	26	11	21.1	265	64	11	21.2
CS02	4	189	45	7	36.4	267	28	7	36.4
CS03	6	167	31	13	19.5	258	48	13	19.4
CS04	7	152	39	10	20.1	281	54	10	20.1
CS05	4	196	11	62	11.7	222	23	62	11.7
CS06	5	186	17	41	12.1	227	34	41	12.1
CS07–08–09	8	201	−4	10	18.7	209	14	10	18.7
Mean	7	178	25	10	19.6	243	41	9	21.7
		Pole: lat = −40, long = 97.6				Pole: lat = −6, long = 40			
		$dp = 11.3$, $dm = 21.1$				$dp = 16.0$, $dm = 26.4$			
		Palaeolatitude: = −13 ± 11.3°				Palaeolatitude: = −23 ± 16.0°			
		Mean corrected for plunge 70° west:				215	41	9	21.7

different ages of magnetization. If the declination difference is due to local rotation, the inclination is still a valid indicator of palaeolatitude. The mean direction of magnetization from locality P39–40 is indicative of a Southern Hemisphere, reversed palaeomagnetic field. The mean direction from locality P41 is also in the appropriate quadrant for a Southern Hemisphere reversed magnetization. The correction for plunge causes the magnetization directions to converge toward a direction which is also consistent with a Southern Hemisphere magnetization. The high blocking temperatures of the characteristic magnetizations and the fact that the inclinations are identical after structural correction leads to the hypothesis that the Kunlun Terrane was in moderate southern latitudes during the Carboniferous.

(ii) *Dykes of the Triassic igneous province* (P32, P42, P43)

In the northern Kunlun a swarm of basalt–andesite dykes cuts the Kunlun batholith. Although the dykes are not directly dated, the petrology indicates they intruded the batholith while the body was still hot (Pearce & Mei, this volume). The Kunlun batholith is dated isotopically at 260–240 Ma (Harris, Xu, Lewis, & Jin, this volume) and the dykes are likely to be in this age range.

Figure 14 illustrates typical thermal demagnetization responses of specimens from these dykes. As illustrated by the behaviour of DK15, DK42 and DK55, a high-temperature component is isolated between temperatures of 500 and 590 °C. This component generally has the same direction as a thermally-distributed magnetization removed at temperatures below 500 °C. Some specimens, like DK20, have only a thermally distributed magnetization which is the same direction as the high blocking temperature magnetizations in other specimens.

Mean site directions, statistics, pole positions and palaeolatitude are summarized in table 11. It is not possible to apply a structural correction to dykes.

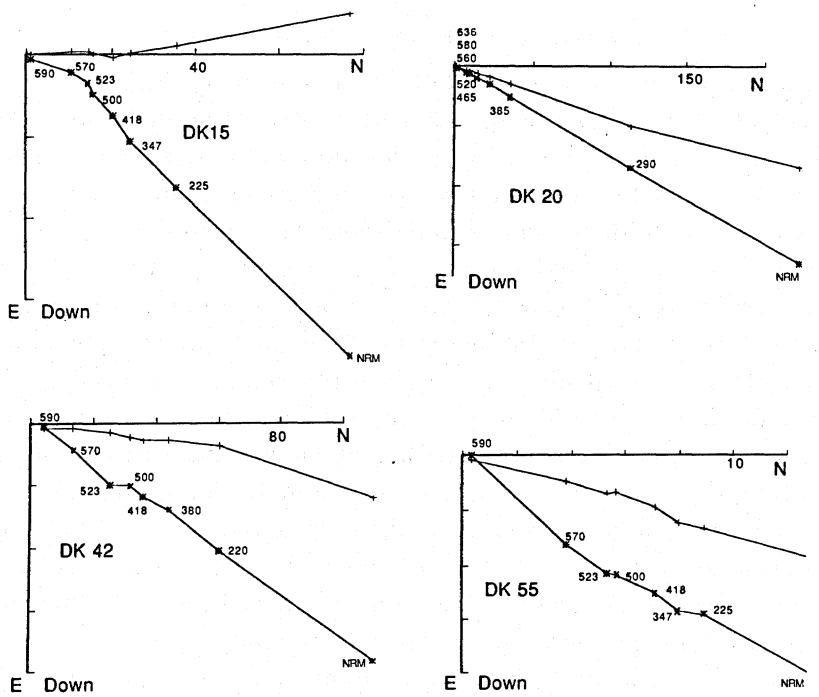

FIGURE 14. Orthogonal projections of thermal demagnetization results from the dykes intruding the Kunlun Batholith. Convention of plotting is as in figure 2.

TABLE 11. DYKES INTRUDING KUNLUN BATHOLITH, MEAN SITE DIRECTIONS, STATISTICS, POLE POSITIONS AND PALAEOLATITUDES

(The arrangement and parameters are as in table 2.)

Unit: Triassic dykes (P32, P42-43)
Location: South of Golmud (36° 10′, 94° 47′)
Age: 240 Ma

site	*N*	*Dec*	*Inc*	*k*	alpha95
DK01	6	18	37	85	7.3
DK02	6	15	36	67	8.2
DK03	3	2	38	40	19.8
DK04	3	3	39	49	17.7
DK05–6	4	5	39	14	26.0
DK07–8	5	12	40	57	10.2
DK10–11	4	17	45	62	11.7
DK12	5	13	41	126	6.9
DK13	4	349	69	5	45.1
DK14–15	4	23	48	63	11.7
DK16	4	17	53	61	11.8
DK17–19	5	8	43	43	11.8
DK20–21	6	4	46	17	16.9
AK01	4	2	37	128	8.1
AK02–3	5	356	34	278	4.6
AK04	5	14	41	160	6.1
Mean	16	9	43	60	4.8

Pole: lat = 76°, long = 237°, dp = 3.7°, dm = 5.9°
Palaeolatitude: = 25 ± 3.7°

PHILOSOPHICAL TRANSACTIONS OF THE ROYAL SOCIETY A MATHEMATICAL, PHYSICAL & ENGINEERING SCIENCES

4. Discussion and conclusions

The present data set from the Tibetan Plateau is too sparse to draw apparent polar wander paths for individual terranes. Even with a much larger set of results, it may prove impossible to do this as local rotations within deformed terranes will obscure palaeoazimuths. Palaeolatitude may be determined from a valid palaeomagnetic mean direction and the analysis of terrane configuration can be done using latitude anomalies, much as Irving (1977) investigated the arrangement of the elements of Pangea. Achache *et al.* (1984) also used a similar approach to examine the position of the Lhasa Terrane relative to Eurasia and India.

Latitude anomalies are calculated using various reference apparent polar wander paths for Eurasia. A palaeolatitude is calculated for a given palaeomagnetic locality using the present latitude and longitude of the site and the pole position with the appropriate age from the reference compilation. From this is subtracted the observed palaeolatitude calculated from the mean palaeomagnetic direction to form the latitude anomaly. Southern latitudes are considered negative so if the latitude anomaly is positive, the terrane is determined to have been south of the calculated latitude. If the site is found to have been north of the calculated position, the latitude anomaly is negative. If the site is determined to have been at the same relative latitude within the Eurasian frame of reference, the latitude anomaly is zero.

The calculation of latitude anomalies is carried out using four separate compilations of the reference apparent polar wander path for Eurasia including those of Irving (1977), Jowett *et al.* (1987) and Westphal *et al.* (1986). Both the 20 Ma and the 30 Ma running average computations of Jowett *et al.* (1987) are used. The Westphal *et al.* (1986) compilation does not include Palaeozoic pole positions. Although results differ somewhat in the value of the latitude anomaly and in the error associated with each result, the latitude anomalies all remain positive.

Table 12 summarizes the results of this calculation for the data from the Tibetan Plateau for each of the reference apparent polar wander paths. Latitude anomaly is plotted as a function of the estimated age of acquisition of the mean direction of magnetization in figure 15 for each of the polar wander paths. The choice of apparent polar wander path does not seem to affect the overall result. The errors of the latitude anomaly are found by adding the error of the relevant pole position to the estimated error, $d\phi$, of the palaeolatitude. Results from each terrane are identified with the appropriate symbols.

The estimate of the latitude anomaly from the Dagangou Formation palaeomagnetic determination for the Carboniferous Kunlun Terrane does have an error of the order of $\pm 25°$, which is a combination of the error of the relevant pole position and the estimate of the error in the palaeolatitude. Even with this error, the latitude anomaly does indicate a position of the Kunlun Terrane well south of its present position relative to Eurasia. The large error in the estimate of the palaeolatitude arises from the small number of sites used for the computation of the mean directions. The difference in the mean declination between the two localities in the Dagangou Formation adds a degree of uncertainty to this result. A correction for a plunge of the folds 70° west brings the declinations closer together to the extent that the cones of 95% confidence for the two localities overlap. The resulting palaeomagnetic directions are definitely of Southern Hemisphere affinity. In view of the uncertainty of the appropriate structural correction, emphasis is placed on the palaeomagnetic inclinations from the Carboniferous results. The magnitude of the latitude anomaly for the Kunlun does indicate that an ocean existed between the Kunlun Terrane and Eurasia with the suture somewhere north of the palaeomagnetic localities investigated in this study.

PHILOSOPHICAL TRANSACTIONS OF THE ROYAL SOCIETY A MATHEMATICAL, PHYSICAL & ENGINEERING SCIENCES

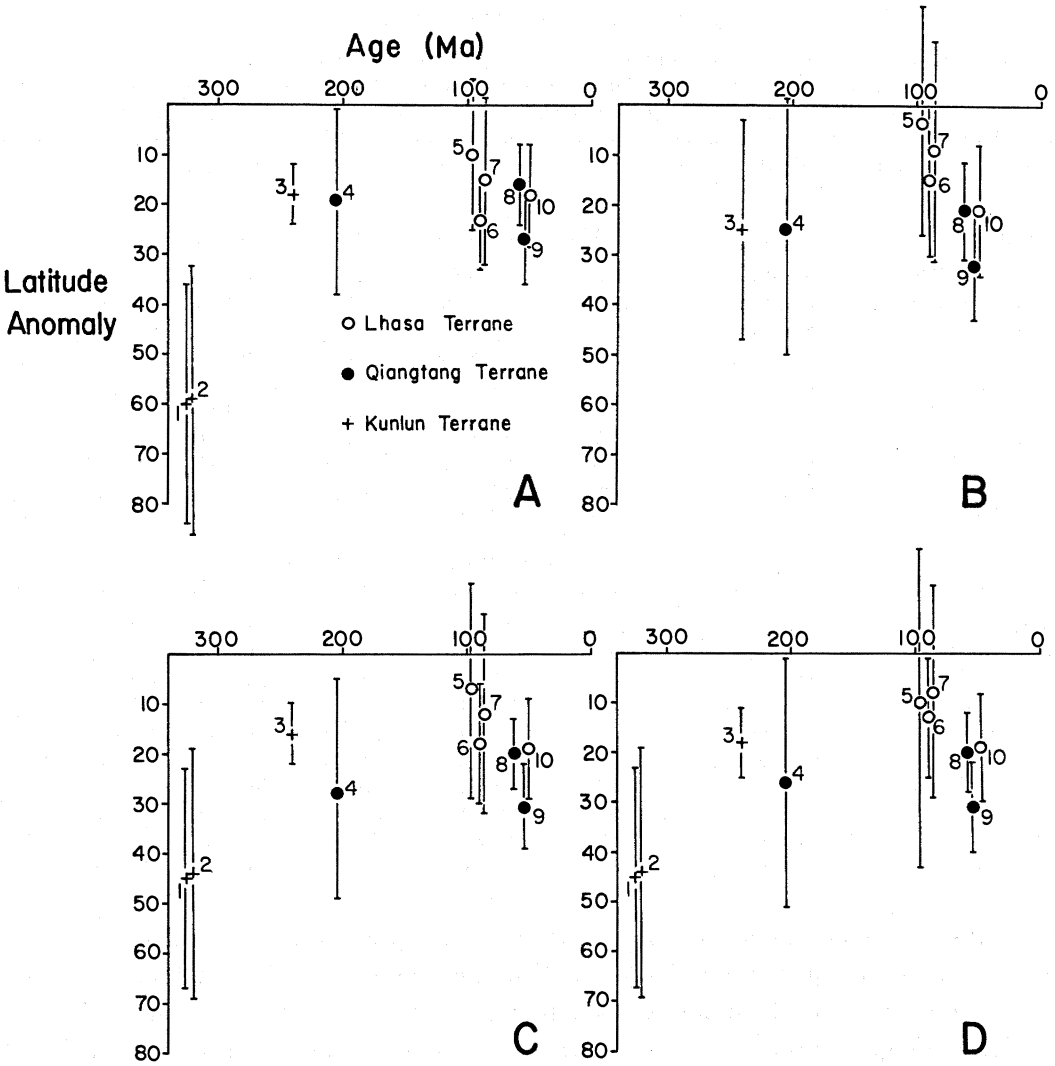

FIGURE 15. Latitude anomalies. The age of the magnetization (in Ma) from which the palaeolatitude determination is made is plotted against the latitude anomaly. The latitude anomalies are calculated from various reference apparent polar wander paths for Eurasia including: Irving (1977); B, Westphal *et al.* (1986); Jowett *et al.* (1987), 30 Ma running average; D, Jowett *et al.* (1987), 20 Ma running average. The individual points are: 1, Dagangou Formation, locality P41; 2, Dangangou Formation, locality P39–40; 3, Dykes intruding Kunlun Batholith; 4, Batang Group volcanics; 5, Nagqu mid-Cretaceous volcanics; 6, Takena Formation redbeds (this study & Achache *et al.* 1984); 7, Qelico mid-Cretaceous volcanics; 8, Fenghuoshan Group, locality P24; 9, Fenghuoshan Group locality P23; 10, Linzizong Group volcanics (Achache *et al.* 1984).

The latitude anomaly for the Kunlun Terrane is reduced to about 20° by the Triassic, if this is indeed the age of magnetization of the basaltic and andesite dykes which cut the Kunlun batholith.

The data from the Batang Group volcanics of Norian age (205 Ma) also indicate a latitude anomaly of about 20°. A direct comparison of the results from this unit with the basalt and andesite dykes cutting the Kunlun batholith is difficult, given the probable difference of 35 Ma between the ages of magnetization. Both determinations show the Kunlun Terrane and the Qiangtang Terrane in the same latitude belt during the Triassic. It is unfortunate that no pre-Triassic magnetizations could be found in the Qiangtang Terrane to test for separation across the Jinsha Suture.

PHILOSOPHICAL TRANSACTIONS OF THE ROYAL SOCIETY A MATHEMATICAL, PHYSICAL & ENGINEERING SCIENCES

TABLE 12. LATITUDE ANOMALIES

(The measured palaeolatitude is determined from the appropriate palaeomagnetic result. The predicted palaeolatitudes (pred) are calculated from the Eurasian apparent polar wander paths of: A, Irving (1977); B, Westphal *et al.* (1986); Jowett *et al.* (1987) 30 Ma running average; D, Jowett *et al.* (1987) 20 Ma running average. The latitude anomaly (anomaly) is determined by subtracting the measured latitude from the predicted latitude. The error is determined by adding the error, dp, of the measured latitude to the error in the appropriate reference palaeomagnetic pole.)

geological unit	terrane	age/Ma	measured latitude	Irving (A) Pred	Irving (A) Anomaly	Westphal (B) Pred	Westphal (B) Anomaly
Dagangou Formation (P39–40)	Kunlun	325	−23±16	37±8	60±24	*****	*****
Dagangou Formation (P41)	Kunlun	325	−22±19	37±8	59±27	*****	*****
Kunlun dykes	Kunlun	240	25±4	43±3	18±7	*****	*****
Batang Group	Qiangtang	205	29±14	47±4	19±18	54±13	25±27
Fenghuoshan Group (P23)	Qiangtang	50	7±4	34±5	27±9	39±7	32±11
Fenghuoshan Group (P24)	Qiangtang	50	18±3	34±5	16±8	39±7	21±10
Nagqu Cretaceous volcanics	Lhasa	96	19±4	36±6	17±10	29±14	10±18
Qelico Cretaceous volcanics	Lhasa	90	20±11	35±6	15±17	29±12	9±22
Takena formation	Lhasa	90	11±4	34±6	22±8	28±12	15±15
Linzizong Formation	Lhasa	50	13±6	31±4	18±10	34±7	21±13

geological unit	terrane	age/Ma	measured latitude	Jowett (C) Pred	Jowett (C) Anomaly	Jowett (D) Pred	Jowett (D) Anomaly
Dagangou Formation (P39–40)	Kunlun	325	−23±16	22±6	45±22	22±6	45±22
Dagangou Formation (P41)	Kunlun	325	−22±19	22±6	44±25	22±6	44±25
Kunlun dykes	Kunlun	240	25±4	41±2	16±6	43±3	18±7
Batang Group	Qiangtang	205	29±14	54±9	28±23	52±11	26±25
Fenghuoshan Group (P23)	Qiangtang	50	7±4	38±4	31±8	38±5	31±9
Fenghuoshan Group (P24)	Qiangtang	50	18±3	38±4	20±7	38±5	20±8
Nagqu Cretaceous volcanics	Lhasa	96	19±4	33±12	14±26	36±24	17±28
Qelico Cretaceous volcanics	Lhasa	90	20±11	32±9	12±20	28±10	8±21
Takena formation	Lhasa	90	11±4	30±9	18±12	26±10	13±12
Linzizong Formation	Lhasa	50	13±6	32±4	19±10	32±5	19±11

The 20° latitude anomaly appears to persist for the Qiangtang Terrane until Palaeocene–Eocene time, or the time of magnetization of the Fenghuoshan Group. The P23 section shows a rather more southerly latitude anomaly than the P24 section. As noted previously, the P23 mean direction of magnetization, before structural correction, is near the present-day field for the central Tibetan Plateau. The mean direction derived from the P23 section is not present field, either before or after structural correction. For this reason, the estimate of the latitude anomaly from the P24 section is probably the more reliable.

The results of Achache *et al.* (1984) showing the Lhasa Terrane about 20° south of its present position within the Eurasian frame of reference are reproduced for the Takena Formation and further supported by the data from the mid-Cretaceous andesites near Qelico.

The contemporaneous magnetizations from the Linzizong volcanics in the southern Lhasa Terrane and the Fenghuoshan Group in the Qiangtang Terrane are directly comparable. Such an exercise shows no resolvable separation in latitude other than what presently exists. Certainly no separation over the Banggong Suture is expected as it was closed by late Jurassic time. More importantly, no north–south crustal shortening is resolved between these two points on the Tibetan Plateau. The early Tertiary estimate of the latitude of Erdaogou is 18±3° and the early Tertiary southern Lhasa Terrane is 13±6°. The difference is close to the present separation of 4° of latitude. The total error on this estimate is 9° or ±1000 kilometres.

Figure 15 shows a persistent 20° southern latitude anomaly for the Tibetan Plateau from the Triassic thorough the Eocene. One interpretation is that each terrane successively accreted to

Eurasia about 20° south of their present locations within the Eurasian frame of reference. They remained at such a position until the Eocene, after which a converging India drove them northward. In the absence of evidence for Eocene ocean crust between the Kunlun Terrane and Eurasia, this process must have involved either shortening of continental crust and/or pushing it out of the way via a Tapponier *et al.* (1982) mechanism. No post-Eocene crustal shortening between the southern Lhasa Terrane and the central Qiangtang Terrane (Erdaogou) is resolved, but the uncertainty is ±9° of latitude or about ±1000 kilometres. An outstanding question that can be addressed by future work in this part of the world is how far northward does the latitude anomaly persist in Asia for rocks of early Tertiary age? Is there an abrupt boundary over which this anomaly disappears or does it vanish gradually as the northward distance from Erdaogou increases?

The Carboniferous Southern Hemisphere, moderate latitude of the Kunlun Terrane is shared by a number of other blocks now incorporated in Asia. These include the South China block (Lin 1984), Iran (Soffel & Forster 1980) and Turkey (Lauer 1984). Palaeomagnetic data do indicate that a considerable amount of continental crust, now incorporated in Eurasia, was in moderate southern latitudes during the Carboniferous. Although it is not possible to use the palaeomagnetic data to constrain the relative positions of these blocks because of the ambiguity in the longitude, a possible reconstruction of these blocks is shown in figure 16, illustrating relative latitude with respect to major continental blocks. The blocks are arranged in longitude according to the minimum movement criteria of Irving (1977). Afghanistan is included in this assemblage of continental crust in moderate southern hemisphere latitudes as the limited data available for only the Permian (Krumsiek 1976) suggest that it was in moderate Southern Hemisphere latitudes during the Upper Palaeozoic. No data for the Palaeozoic are available for the Qiangtang Terrane or the Lhasa Terrane. The Qiangtang Terrane is positioned near the Kunlun Terrane as the palaeontological data (Smith & Xu, this volume) do

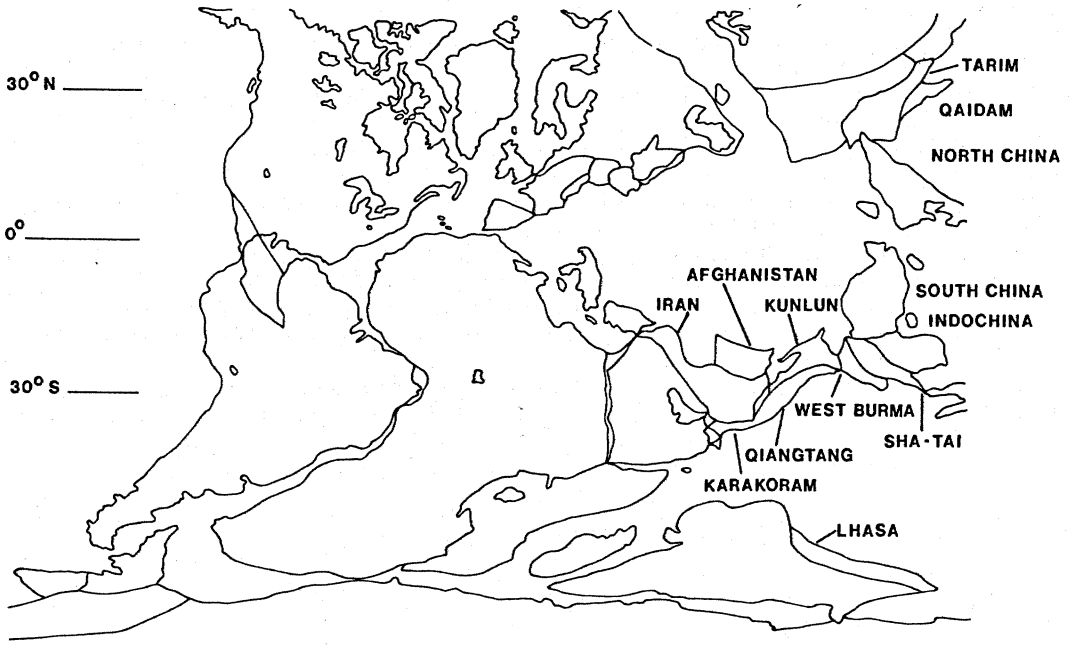

FIGURE 16. Upper Palaeozoic (Carboniferous) palaeogeographic reconstruction showing location of various southern Asian blocks with respect to major continents.

not suggest a substantial difference in palaeolatitude. The Lhasa Terrane is shown in a high southern latitude as suggested by the occurrence of the Carboniferous mixtites. As only the latitudes of these blocks are constrained, and a considerable difference in longitude could exist, the continuity implied by figure 16 must be tested by palaeontological methods.

We thank Professor J. C. Briden for making the laboratory facility at the University of Leeds available for the measurements of the samples. Sample preparation and measurement were supported by the Natural Environmental Research Council. K. Roberts assisted in the measurement of the samples. R. Cumberland helped with the transfer of computer files. A. G. Smith kindly provided computer facilities.

References

Achache, J., Courtillot, V. & Xu, Z. Y. 1984 Paleogeographic and tectonic evolution of southern Tibet since Middle Cretaceous time: New paleomagnetic data and synthesis. *J. geophys. Res.* **89**, 10311–10339.

Chang Chengfa and 26 others 1986 Preliminary conclusions of the Royal Society and Academia Sinica 1985 geotraverse of Tibet. *Nature, Lond.* **323**, 501–507.

Coulon, C., Maluski, H., Bollinger, C. & Wang, S. 1986 Mesozoic and Cenozoic volcanic rocks from central and southern Tibet: $^{40}Ar/^{39}Ar$ dating, petrological characteristics and geodynamical significance. *Earth planet. Sci. Lett.* **79**, 281–302.

Halls, H. 1978 The use of converging remagnetization circles in paleomagnetism. *Phys. Earth Planet Int.* **16**, 1–11.

Irving, E. 1977 Drift of the major continental blocks since the Devonian. *Nature, Lond.* **270**, 304–309.

Jowett, E. C., Pearce, G. W. & Rydzewski, A. 1987 A mid-Triassic paleomagnetic age of the Kupferschiefer mineralization in Poland based on a revised apparent polar wander path for Europe and Russia. *J. geophys. Res.* **92**, 581–598.

Kent, J. T., Briden, J. C. & Mardia, K. V. 1983 Linear and planar structure in ordered multivariate data as applied to progressive demagnetization of palaeomagnetic remanence. *Geophys. Jl R. astr. Soc.* **75**, 593–620.

Krumsiek, K. 1976 Zur Bewegung der Iranish–Afghanischen Platte. *Geol. Rundsch.* **65**, 908–929.

Lauer, J. P. 1984 The geodynamic evolution of Turkey and Cyprus in the light of recent palaeomagnetic data. In *The geological evolution of the Eastern Mediterranean* (ed. J. E. Dixon & A. H. F. Robertson). *Spec. Publ. Geol. Soc. London* **17**, 483–491.

Lin, J. L. 1984 The apparent polar wander paths for the North and South China blocks. Ph.D. thesis, University of California, Santa Barbara.

McElhinny, M. W. 1966 An improved method for demagnetizing rocks in alternating magnetic fields. *Geophys. Jl R. astr. Soc.* **10**, 369–374.

McElhinny, M. W., Luck, G. G. & Edwards, D. 1971 A large volume magnetic field-free space for thermal demagnetization and other experiments. *Pure appl. Geophys.* **80**, 127–130.

Soffel, H. C. & Forster, H. G. 1980 Apparent polar wander path of central Iran and its geotectonic interpretation. *J. Geomagn. Geoelect.* **32** (suppl. III), 117–135.

Tapponnier, P., Peltzer, G., Le Dain, A. Y., Armijo, R. & Cobbold, P. 1982 Propagating extrusion tectonics in Asia: new insights from simple experiments with plasticine. *Geology* **10**, 611–616.

Westphal, M., Bazhenov, M. L., Lauer, J. P., Pechersky, D. M. & Sibuet, J. C. 1986 Paleomagnetic implications on the evolution of the Tethys Belt from the Atlantic Ocean to the Pamirs since the Triassic. *Tectonophysics* **123**, 37–82.

Zijderveld, J. D. A. 1967 A. C. demagnetization of rocks: Analysis of results. In *Methods in palaeomagnetism* (ed. D. W. Collinson, K. Creer & S. K. Runcorn), pp. 254–286. Elsevier: Amsterdam.

PHILOSOPHICAL TRANSACTIONS OF THE ROYAL SOCIETY A MATHEMATICAL, PHYSICAL & ENGINEERING SCIENCES